PAPER • **OPEN ACCESS**

Solvent-based revival of carbon-based perovskite solar cells

To cite this article: Elena S Akulenko *et al* 2026 *Eng. Res. Express* **8** 125322

Engineering Research Express

OPEN ACCESS

RECEIVED
30 March 2026

REVISED
20 May 2026

ACCEPTED FOR PUBLICATION
26 May 2026

PUBLISHED
19 June 2026

PAPER

Solvent-based revival of carbon-based perovskite solar cells

Elena S Akulenko[1,*], Mahboubeh Hadadian[1], Anna Knol[1], Simon Jech[2], Sirius Yli-Paavola[1], Annukka Santasalo-Aarnio[2] and Kati Miettunen[1]

[1] Department of Mechanical and Materials Engineering, Facility of Technology, University of Turku, Turku FI-20014, Finland
[2] Department of Energy and Mechanical Engineering, School of Engineering, Aalto University, PO Box 16100, 00076 Aalto, Finland
[*] Author to whom any correspondence should be addressed.

E-mail: elena.akulenko@utu.fi

Keywords: revival, perovskite solar cells, recycling, γ-valerolactone, eco-design, sustainability

Supplementary material for this article is available online

Abstract

Perovskite solar cells (PSCs) combine high efficiency with low-cost processing, but their rapid progress toward commercialization is challenged by insufficient end-of-life strategies. Here we present the proof-of-concept of solvent-based revival of carbon-based PSCs using the green solvent γ-valerolactone (GVL) reaching high revival rates, which requires significantly less energy compared to the production of a new device. With this revival approach, we not only recover the materials but also the structure of the whole devices, including the energy and costs invested in them in the original manufacturing, thus advancing the highest level of resource-efficient recycling within the eco-design concept. Devices subjected to the optimized protocol revived up to 95% of their initial power conversion efficiency, with a stable fill factor and only modest reductions in photocurrent and open-circuit voltage (V_{oc}). Impedance spectroscopy revealed only a small increase in series and charge-transfer resistances, attributable to interfacial changes of the carbon/perovskite boundary, while scanning electron microscopy confirmed the preservation of the carbon scaffold and successful reinfiltration of the perovskite precursor. Energy return on investment analysis further highlighted the sustainability advantage of revival compared to single-use devices. These results establish GVL-assisted revival as a practical first-level recycling strategy for PSCs.

1. Introduction

PSCs have rapidly emerged as one of the most promising photovoltaic (PV) technologies, achieving power conversion efficiencies of 27% in single-junction devices and 30.1% in perovskite–perovskite double junction devices (NREL Best Research-Cell Efficiencies Chart 2025). Their combination of high performance, low-temperature solution processing, and compatibility with lightweight and flexible substrates has positioned PSCs as strong candidates for next generation solar technologies with commercial potential (Sengupta *et al* 2025). With the growing attention to scaling strategies (Li *et al* 2025), the urgency of addressing end-of-life (EoL) strategies is increasing. Regulatory and environmental frameworks such as the EU Waste Electrical and Electronic Equipment Directive and restrictions on hazardous substances highlight the need for sustainable management of toxic lead and electronic waste.

Despite these drivers, research on PSCs remains dominated by efficiency and operational stability studies, while sustainable EoL strategies lag behind. In our previous work, we introduced an eco-design concept that classifies PV recycling into four levels depending on the balance between energy input and value output: (i) reviving a device, (ii) reusing components, (iii) recycling compounds, and (iv) recovering elements (Miettunen and Santasalo-Aarnio 2021). Traditionally PSCs recycling efforts have been focused on full recovery of valuable materials, which is called recycling-remake strategy (Binek *et al* 2016, Kadro and Hagfeldt 2017, Wang *et al* 2021). Under this approach the whole device architecture is mechanically and chemically disassembled to separate and individually recycle the materials for further reuse. Recent advances in PSC recycling have mainly addressed the middle levels. Holistic aqueous (Xiao *et al* 2025) and solvent-based circular recovery (Larini *et al* 2025) enable high-purity material reuse

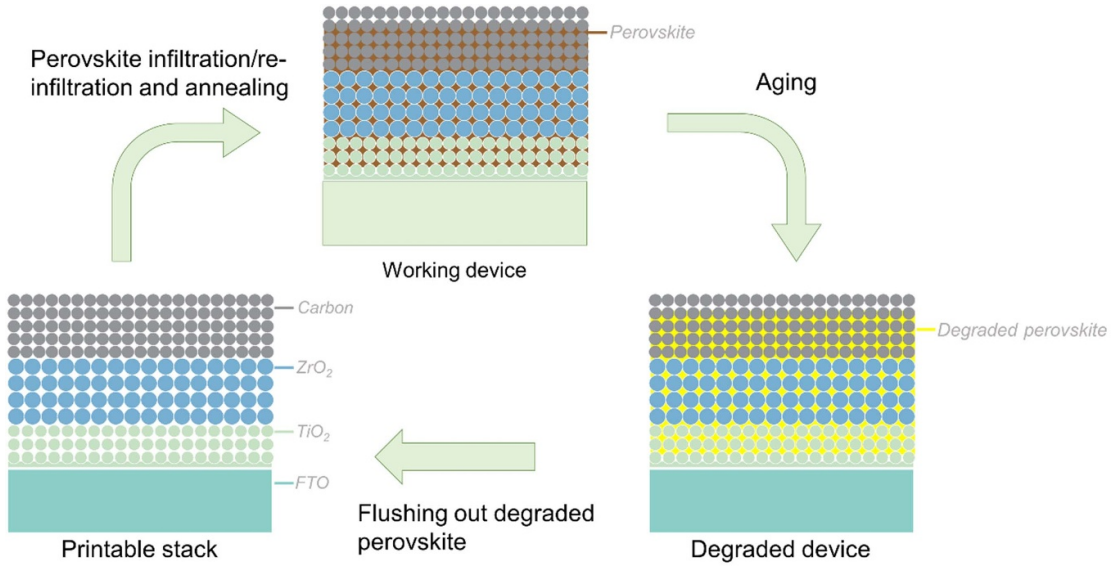

Figure 1. C-PSCs device-level revival within the circular economy concept (reproduced from Hadadian *et al* 2025). To begin with, a printable stack is prepared where perovskite is infiltrated to make a working device, which then be used. At the end of life, the perovskite can be flushed out from the degraded device to have the stack ready for another perovskite infiltration.

while lowering cost and environmental impact. Green solvent approaches (Pacchioni 2025) and recent reviews (Selvanathan *et al* 2025) confirm the potential of low-toxicity strategies, though challenges with encapsulation, scalability, and lead safety remain. These developments strengthen the intermediate levels of the eco-design concept (i.e. component reuse and compound recycling). The revival level—restoring device performance without destroying the architecture—represents the most resource-efficient strategy but remains largely unaddressed.

In our previous contribution, we showcased what these recycling levels options could entail for perovskite solar cells and their technoeconomic assessment (Akulenko *et al* 2023). In that study, we highlighted that among different PSC architectures, mesoporous PSCs, in particular carbon-based PSC (C-PSCs) are promising in this respect. In C-PSCs, the photoactive material, perovskite, is the material that is the most susceptible to degradation (Zouhair *et al* 2024). Perovskite is infiltrated in the mesoporous C-PSCs scaffold, providing a unique feature for washing off the perovskite from the scaffold at the end of life and reinfiltrate new (or regenerated) perovskite, which is called reviving the whole device (figure 1). Beyond their recyclability, C-PSCs are especially attractive due to their low-cost materials, facile fabrication without the need for vacuum deposition or noble metals, and superior long-term stability under ambient conditions. The use of carbon as the back electrode eliminates the need for costly and unstable hole transport layers and gold contacts, making C-PSCs one of the most scalable and commercially relevant architectures for large-area and sustainable perovskite PVs (Hadadian *et al* 2020, Bogachuk *et al* 2022). A current research question with C-PSC devices is increasing their efficiency (He *et al* 2025).

As we highlighted before, the revival of whole devices is possible with minimal additional energy input (Akulenko *et al* 2023). However, systematic studies on revival remain scarce. Existing demonstrations include revival of C-PSCs via methylamine gas treatment (Hong *et al* 2017) and solvent-based approaches applied to devices with metallic electrodes (Zhiliang Ku *et al* 2015). Gas-based processes add complexity and bring additional safety concerns, making solvent based processing more preferred from both practical and environmental perspectives.

Despite this potential, solvent-based revival specifically for C-PSCs has received very limited attention in the literature. In our previous work, we reported an initial proof-of-concept for solvent-based revival of C-PSCs and compared N,N-dimethylformamide (DMF), dimethyl sulfoxide (DMSO), and γ-valerolactone (GVL), but the revival rates were modest (∼65%) (E. Akulenko *et al* 2023). While DMF and DMSO readily dissolved perovskite, they frequently induced peeling of the carbon mesoporous layer. GVL, in contrast, effectively dissolved degraded perovskite with minimal or no carbon peeling, showing more promise for perovskite revival (E. Akulenko *et al* 2023).

This behavior can be rationalized by differences in solvent properties. As summarized in table 1, DMF and DMSO exhibit high dielectric constants, high donor numbers, and high PbI_2 solubility resulting in strong coordination with Pb^{2+}, though this strong interaction also leads to mechanical stress on

Table 1. Key solvent properties relevant for solvent-based revival of C-PSCs.

Solvent	Chemical structure	Dielectric constant ε (25 °C)	Donor number (DN)	PbI_2 solubility (30 °C)	Hansen δD, δP, δH ($MPa^{1/2}$)	Key features and environmental aspect	References
DMF	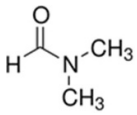	36.7	26.6	Very high (⩾2 M)	17.4 13.7 11.3	Strong Pb^{2+} coordination; aggressive towards carbon scaffold; reprotoxic solvent; SVHC under EU REACH; unsuitable for sustainable scale-up	(Prat *et al* 2014, Petrov *et al* 2021)
DMSO	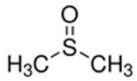	46.7	29.8	High (⩾1.4 M)	18.4 16.4 10.2	Very strong Pb^{2+} coordination; induces carbon peeling; low acute toxicity solvent	(Prat *et al* 2014, Petrov *et al* 2021)
GBL	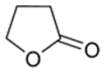	42	18	Sufficient*	18.0 16.6 7.4	Used as common perovskite precursor solvent; low coordination strength; petrochemical origin; regulatory and toxicity concerns limit sustainability	(Stevenson *et al* 2017, Radicchi *et al* 2020, Petrov *et al* 2021)
GVL	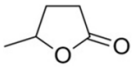	36.0	>18**	Sufficient***	17.1 11.9 6.2	Moderate coordination; preserves carbon scaffold; bio-based, biodegradable, low-toxicity solvent; aligned with sustainability principles	(Kerkel *et al* 2021, Worsley *et al* 2021, Akulenko *et al* 2023, Miao *et al* 2023, Väisänen 2025)

*Sufficient to dissolve precursors in typical perovskite formulations (Petrov *et al* 2021).

**We note that, unlike DMF and DMSO, an experimentally determined DN for GVL has not been reported in the literature. Therefore, comparison with gamma-butyrolactone (GBL) provides a useful benchmark. Worsley *et al* (2021) suggests that GVL coordinates more readily to Pb^{2+} centers compared to GBL (DN = 18).

***Sufficient solubility demonstrated by complete removal of degraded perovskite and successful reinfiltrating (E. Akulenko *et al* 2023).

mesoporous carbon layer. GVL, in contrast, exhibits moderate coordination to Pb^{2+}, offering comparable to DMF dielectric constant. This balance appears sufficient to dissolve degraded perovskite while limiting mechanical stress on the mesoporous carbon electrode, as reflected by the substantially reduced carbon peeling observed experimentally (E. Akulenko *et al* 2023). In addition, GVL is a bio-based, low-toxicity solvent, making it particularly attractive in terms of environmental and sustainability aspects. Recently, a GVL-based remanufacturing potential for mesoscopic C-PSCs was investigated. However, the reported results do not directly quantify the extent to which the functionality of an individual cell can be restored after perovskite washing out (Valadez-Villalobos *et al* 2025). A critical issue remaining largely unexplored in the literature is reaching high revival rates with C-PSCs using a solvent-based revival strategy.

The present study provides the proof-of-concept of high revival rates of C-PSCs using a green solvent, GVL, fully aligned with circular economy principles complemented with energy investment analysis. The optimized protocol, incorporating simplified handling to reduce electrode damage, enabled an average revival rate of 95% of the initial power conversion efficiency across multiple devices. In addition to investigating the PV performance of the devices of original and revived devices, their conductivity is studied using electrochemical impedance spectroscopy (EIS). Furthermore, the morphology

of the carbon layer before and after revival is investigated using scanning electron microscope (SEM). Photoluminescence (PL) measurements were also performed to verify whether the revival step preserved the characteristics of the perovskite absorber. To contextualize the energy implications of revival, we refer to the concept of energy return on investment (EROI) (Celik *et al* 2018), which compares the net energy gained with the net energy invested to providing an energy source (Murphy and Hall 2010, Arvesen and Hertwich 2015, Jech *et al* 2026). While traditionally applied to first-use devices, this concept can also be extended to evaluate the benefits of revival, where single-use devices are compared with revived ones as done in this study.

2. Materials and methods

The study combined fabrication of C-PSCs, their solvent-assisted revival with GVL, and subsequent performance, electrical, and morphological characterization. In addition, EROI analysis was applied to evaluate the sustainability benefits of device revival relative to first-use operation.

2.1. Materials

For fabricating C-PSCs a complete commercial kit of components from Solaronix was used. The primary aim of the present work was to demonstrate that high revival rates for C-PSCs can be reached under well-defined and simplified conditions. Therefore, we prioritized the use of commercially available materials, which have well-defined and reproducible characteristics. The kit included prefabricated carbon monolithic electrodes (CME), ready-to-use perovskite precursor solution and polyamide impregnation masks. CME consisted of a layered structure deposited on fluorine-doped tin oxide (FTO) glass, comprising a mesoporous ZrO_2 layer, a mesoporous TiO_2 layer, a compact TiO_2 layer and a carbon layer. The precursor solution included lead iodide (PbI_2), methylammonium iodide (CH_3NH_3I), and 5% 5-ammonium valeric acid iodide (5-AVAI) dissolved in GBL. Ethanol (anhydrous, $\geqslant$99.5%) and GVL (anhydrous, 99%) for revival step were purchased from Sigma Aldrich.

2.2. Fabrication process

High-temperature treatment of CMEs was carried out at 400 °C using a programmable hot plate with a closed lid for 30 min after a 30 min ramp. A uniform thermal environment facilitates reaching high performance and removal of the contaminants trapped in the porous structure during storage.

After the heat process, CMEs were allowed to cool down inside the hot plate with a closed lid. Once the temperature dropped to 150 °C, the samples were removed one at a time from under the hot plate lid for masking in a fume hood and immediately returned after. This procedure was repeated sequentially for each CME, ensuring that all the electrodes remained covered by the hot plate lid throughout the cooling process.

Afterward, the mesoporous layers of CMEs were infiltrated with 5.76 μl of methylammonium lead iodide ($MAPbI_3$) precursor solution inside a glovebox. The samples were left in the plastic container with lid on and kept inside the glove box for 30 min to allow the solution uniformly spreads over the electrodes. Then samples were heated at 50 °C for 15 min on a hot plate.

2.3. Revival process

In our initial study of C-PSC (E. Akulenko *et al* 2023), the revival rate was relatively low and various results indicated that the carbon layer is very prone to damage. Thus, here the revival procedure was simplified to reduce handling steps and improve reproducibility compared with our earlier protocol (E. Akulenko *et al* 2023). The key issues in the optimization of the device preparation were to (1) minimize contamination (e.g. by ambient moisture and air) while (2) minimizing the number of heat treatments. Specifically, we modified the masking step to prevent moisture absorption by the porous carbon layer, with detailed procedure given in section 2.2. Then, high temperature treatments were limited to one with high uniformity (note that uncovered hotplate tends to be too unrepeatable) and time from there to the masking was minimized.

No intentional aging or accelerated degradation (e.g. thermal, light-induced, humidity-driven, or combined stress) was applied to the devices prior to revival. The revival protocol was investigated on freshly fabricated devices and on samples in which the perovskite absorber had been removed during the washing-out step.

The actual revival process consisted of immersing the samples in flat beakers with 30 ml of GVL for 30 min at ambient temperature (following the Ku *et al* 2015), continued with ethanol washing, thermal treatment on a hot plate at 150 °C for 10 min, and reinfiltration with the $MAPbI_3$ precursor in a glove

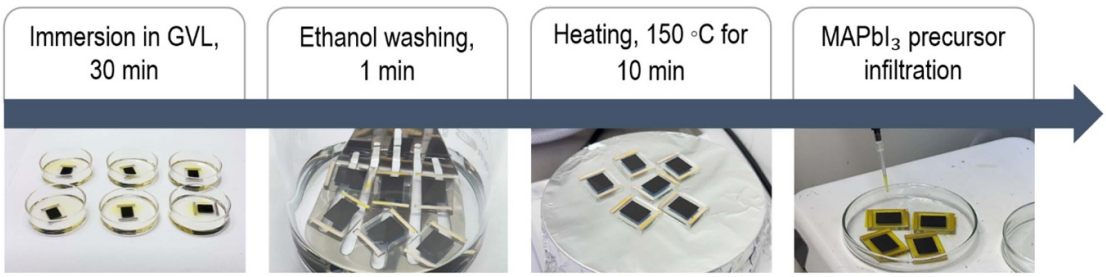

Figure 2. Revival process: step-by-step process for reviving the C-PSCs, washing and reinfiltration of $MAPbI_3$ precursor. Devices are first immersed in GVL, followed by ethanol washing. The substrates are then heated at 150 °C before infiltration with the $MAPbI_3$ precursor solution.

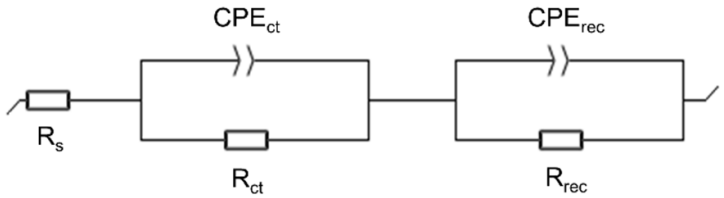

Figure 3. Equivalent circuit diagram, where R_s—the series resistance of carbon electrode and FTO, R_{ct}—the charge transfer resistance at the carbon/perovskite interface, R_{rec}—the charge recombination resistance at the TiO_2/perovskite interface.

box after cooling (figure 2). Variation of GVL volume between 17.5 and 30 ml did not lead to systematic changes in revival efficiency.

For the ethanol washing step, an 800 ml glass beaker containing 200 ml of ethanol was used. The samples were placed on a flat spatula (as shown in figure 2) and gently immersed in the ethanol bath for 1 min at the ambient temperature. After immersion, the samples were lifted using the spatula and immediately transferred onto a hot plate using tweezers.

Further optimization compared to our previous protocol (E. Akulenko *et al* 2023), where samples were immersed in GVL in deep beakers, ethanol washing involved sequential transfer with tweezers across three separate beakers and standard current–voltage (IV) characterization was employed after the washing step, here we simplified the procedures: flat beakers were used for GVL immersion step, and a single wide beaker with a flat spatula was used for ethanol washing to minimize mechanical stress on the carbon electrode, and a multimeter-based check replaced full IV testing. These changes in protocol reduced handling steps and lowered the risk of carbon electrode peeling. Furthermore, it is also more cost-effective, since a method with fewer operations is inherently easier and cheaper to implement on an industrial scale.

2.4. Samples characterization

The performance of the solar cells was measured the next day after fabrication/revival using a solar simulator (PEC-L01, PECCELL) comparable to AM 1.5G standard testing conditions. Prior to the IV measurements, the cells were illuminated under the solar simulator for 1 min. The IV characteristics were recorded with a Gamry Reference 600+ potentiostat, starting from −0.2 V after a 3 s equilibration, and scanned in both forward and reverse directions up to 1 V at a scan rate of 100 mV s^{-1} with a 20 mV step size. IV measurements were performed using a custom mask with a rectangular aperture 0.64 cm^2, smaller than active device area (12.5 × 12 mm^2, fabricated following the protocol of García *et al* (2024).

For the rapid verification of the samples state after ethanol washing, a multimeter-based check was performed using a UNI-T UT133A digital device under ambient light. In these conditions, the samples from which perovskite had been removed typically showed V_{oc} values between 30–40 mV while working devices gave V_{oc} values of 470–560 mV confirming the loss of PV activity.

EIS measurements were conducted with the same Gamry Potentiostat and using the same solar simulator as the light source as in the IV measurements. EIS was carried out in the frequency range from 50 mHz to 5 MHz at zero applied voltage. Data was analyzed using the BioLogic EC-Lab® V11.52 software and fitted to the equivalent circuit diagram shown in figure 3 to obtain impedance parameters.

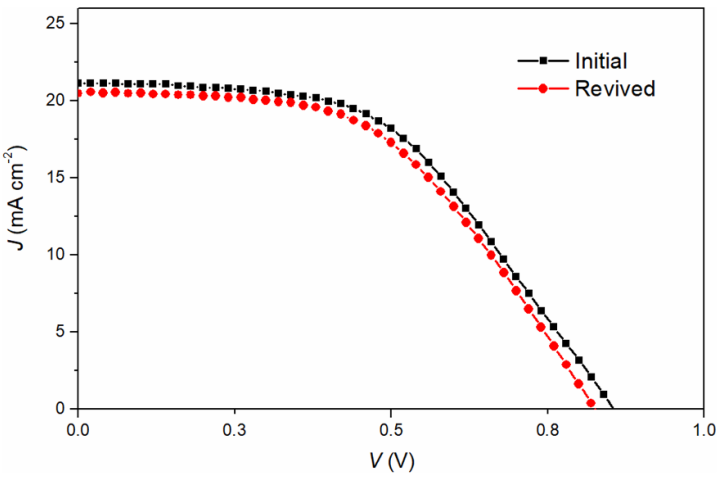

Figure 4. IV curves of a sample before and after revival (reverse scans).

The morphology and elemental composition of the samples was analyzed by SEM (Thermo Scientific Apreo S) and energy dispersive x-ray spectroscopy (EDS) (Oxford Instruments Ultim Max 100 spectrometer). SEM analysis was done at 2 kV and 25 pA, using both Everhart–Thornley (ETD) and the lower in-lens (T1) detectors with a 10 mm working distance. EDS analysis was done at 7 kV and 0.8 nA with the same 10 mm working distance. EDS spectra were analyzed with the AZtec 6.1. software.

Steady-state PL spectra were recorded using an FLS1000 spectrofluorometer (Edinburgh Instruments from UK). Time-resolved PL (TRPL) were carried out using a PicoQuant time-correlated single photon counting setup, and the decay traces were acquired using EasyTau 2.3 software.

2.5. EROI analysis

EROI was utilized to compare the benefits of revival with those of manufacturing new cells. This approach visualizes both the influence of the first operational lifetime and the extended lifetime enabled after revival, allowing the impact of efficiency retention to be analyzed. EROI was calculated in following way:

$$EROI = \frac{E_{\text{Out\_initial}} + E_{\text{Out\_revived}}}{E_{\text{manufacturing}} + E_{\text{revived}}} \quad (1)$$

where $E_{\text{Out\_initial}}$ and $E_{\text{Out\_revived}}$ are the electricity produced by the initial cell and revived cell, respectively. $E_{\text{manufacturing}}$ and E_{revival} are the energy consumed during manufacturing and revival, respectively (detailed break-down in supplementary table S1). The electricity production was calculated:

$$E_{\text{Out}_{\text{first}}} = I \cdot A \cdot UF \cdot t \cdot \eta_{\text{initial}} \quad (2)$$

where I is the average yearly insolation (assumed as 1700 kWh m^{-2} per year (Celik *et al* 2018), A is the active area of the cell (assumed as 1 m^2), UF is the utilization factor (here UF = 0.8), and t stands for years during initial operation ($t = 5$). η_{initial} is the efficiency of the device during first life. Initial efficiency is set to the average measured efficiency of the initial cells at t = 0 and then it was set to linearly decrease to 80% of the initial efficiency at $t = 5$ years. $E_{\text{Out\_revived}}$ was calculated in similar fashion only the efficiency was the respective revived efficiency. The second life efficiency was set to decrease in same fashion as the first life efficiency.

3. Results and discussion

3.1. Samples performance before and after revival

C-PSCs samples fabricated with CMEs were subjected to the optimized GVL-based revival protocol, and their PV performance was assessed before and after revival. Representative IV curves (figure 4) and PVs characteristics (table 1) demonstrate that the overall device functionality was mainly preserved after revival, with only a mild reduction in photocurrent density and open-circuit voltage, while fill factor (*FF*) remained stable.

Table 2. Average photovoltaic characteristics and their standard deviations (for batch 1) at their initial state and after revival.

Cells	Scan direction	J_{sc} (mA cm^{-2})	V_{oc} (V)	*FF* (%)	PCE (%)	Revival rate (%)
Initial	Forward	21.5 ± 0.3	0.83 ± 0.02	40 ± 7	7 ± 1	
	Reverse	21.3 ± 0.4	0.84 ± 0.02	51 ± 1	9.0 ± 0.2	
Revived	Forward	20 ± 1	0.80 ± 0.02	42 ± 2	6.7 ± 0.6	95 ± 20
	Reverse	20 ± 1	0.82 ± 0.02	50 ± 1	8.2 ± 0.5	91 ± 7

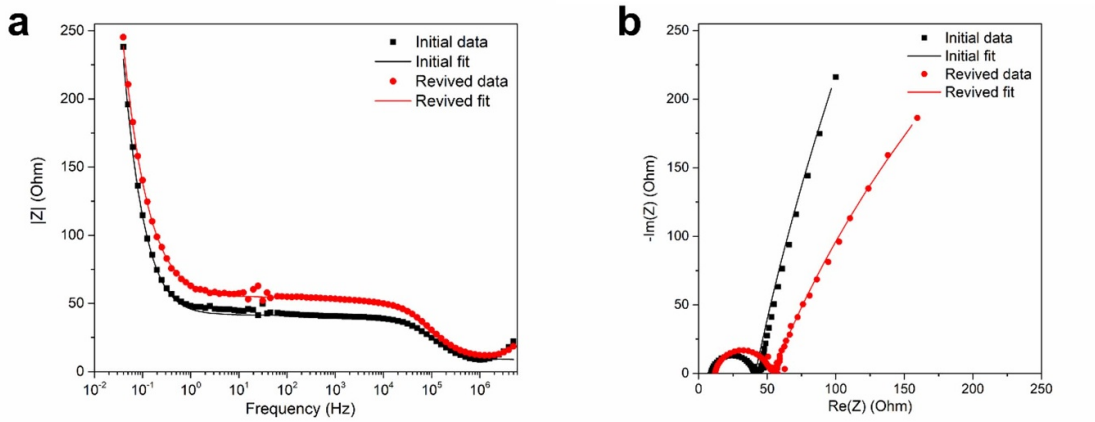

Figure 5. (a) Example Bode plot of the impedance measurements; (b) example Nyquist plot of the impedance measurements.

Initial devices showed average efficiencies of 9.0 ± 0.2% in reverse scans and 7 ± 1% in forward scans. These efficiencies are typical for such simplistic material combination (Grancini *et al* 2017). The more interesting and important part was that after revival, the efficiencies were 8.2 ± 0.5% and 6.7 ± 0.6%, corresponding to revival rates 91% and 95%, respectively. There were only small efficiency (PCE) losses, which are primarily attributed to a drop in short-circuit current (J_{sc}) and in V_{oc} (table 2). These small changes likely originate from incomplete regeneration of the perovskite absorber and interfacial modifications. The *FF* remained largely unaffected as indicated by table 2, which suggests that charge extraction and contact quality were maintained. These results also motivate further studies to reach optimized material combination for high initial performance.

Calculated revival rates (table 2) averaged 95% for forward scans and 91% for reverse scans demonstrate promising revival across the multiple samples. In cell 4 (table S2), the revival performance even exceeded the initial value (7.51% revived vs 5.13% initial), likely due to improved redistribution of the perovskite precursor within the porous carbon scaffold during reinfiltrating. To assess the repeatability of the revival process, we made further batches and the performance data is shown in supplementary table S2. While there is some batch-to-batch variation in original performance as typical, the revival rates were similar in the tested batches. The overall average revival efficiency increases to 96% ± 20 for the forward scan and 92% ± 10 for the reverse scan (table S2). Furthermore, when outlier samples (both outstandingly high and low) are excluded, the overall average revival efficiency is 92% ± 14% for the forward scan and 91% ± 15% for the reverse scan. These results show a substantial improvement compared with our initial study (E. Akulenko *et al* 2023). The higher revival rates can be attributed to protocol simplifications that reduced mechanical stress on the carbon electrode and minimize unnecessary handling steps. Together, these findings confirm that GVL enables efficient and promising revival of C-PSCs, achieving revival rates up to 95% of the initial cells performance (see table 2). This demonstrates the potential of solvent-based revival as a practical first-level recycling strategy within circular economy concept.

3.2. Electrochemical impedance analysis before and after revival

EIS was performed to investigate the impedance characteristics of perovskite solar cells before and after revival. The measurements were done under illumination at 0 V conditions. The Nyquist plot and Bode phase diagram of a device before and after revival are shown in figure 5.

Two arcs can be observed in the Nyquist plot. The semicircle in the high-frequency region is commonly attributed to the R_{ct}, while the low-frequency region shows a part of a parabola associated with

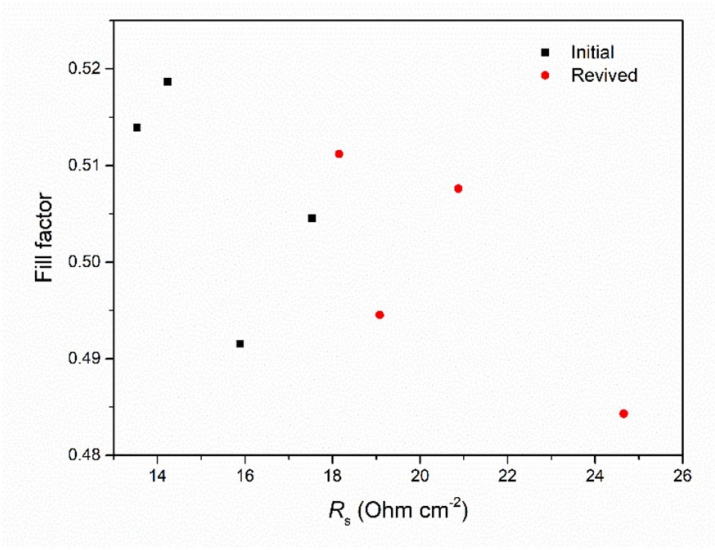

Figure 6. Fill factor vs series resistance R_s.

the R_{rec} (Rong *et al* 2014, Meng *et al* 2018, Don *et al* 2023). Another interesting value is the R_s, which can be read from the distance of the first semicircle from the origo. R_s consists mainly of the sheet resistance of the FTO glass and the carbon layer. The Bode magnitude plot shows that the revival did not affect the time constants of the charge transfer and recombination processes, as both the initial and revived curves plateau and peak at the same frequencies.

Series resistance values increased after the revival process for all the cells, with initial and revived R_s values being 15 $\pm$ 1 Ohm cm^{-2} and 21 $\pm$ 3 Ohm cm^{-2}, respectively. Generally, higher R_s value results in reduced *FF* and thus leads to lower efficiencies (Meng *et al* 2018, Bhandari *et al* 2020). In this study, a statistically significant change in R_s values was noted but the difference is so small that it has only a minor impact on *FF* (figure 6) and consequently on PCE when its increase is calculated (data not shown). This analysis based on EIS is well in line with the IV measurements discussed in the previous section.

Moreover, there was an increase of the R_{ct} at the perovskite/carbon interface after the revival, indicated by the parabolas in the high-frequency region. Average R_{ct} values at the carbon/perovskite interface for initial and revived cells were 60 $\pm$ 10 Ohm cm^{-2} and 68 $\pm$ 4 Ohm cm^{-2}, respectively (table 3). Higher R_{ct} indicates a more hampered transport of holes from the perovskite to the carbon electrode (Don *et al* 2023). However, the changes in R_{ct} cannot be directly compared since the voltage over the photoelectrode is different in different cells due to varying V_{oc} and FF. R_s does not vary based on device voltage, thus allowing reliable comparison. The increase in R_s and potentially R_{ct} could be attributed to minor degradation of the carbon electrode and subsequent changes at the carbon/perovskite interface after the revival process. Results from the fitting of impedance data show that recombination resistance R_{rec} decreased after the revival. Lower R_{rec} values signify faster charge recombination at the TiO_2/perovskite interface which leads to lower V_{oc} values (Don *et al* 2023). This corresponds to the slight drop in V_{oc} observed during IV measurements of the revived cells (table 2).

3.3. Surface morphology analysis

The morphology of the sample surface was analyzed using SEM (figure 7). Top-down images of the initial and revived samples were taken using both the ETD and the T1 detectors. The images taken with the ETD detector show the surface topography of the sample, whereas the T1 images highlight the materials contrast with lighter elements showing darker areas in the images. In the initial samples, the surface appears uniform, with perovskite formation primarily within the carbon electrode. In the T1 image the perovskite formations are seen as lighter spots in the darker carbon electrode surface, but in the ETD image the surface seems uniform and there are no separate perovskite crystal formations on top of the carbon layer. In some of the revived samples, in addition to the formation of the perovskite in the carbon scaffold, perovskite crystal formations are observed on top of the carbon, indicating that some perovskite now forms on the surface rather than within the carbon scaffold. However, figure S1 shows the SEM of another revived cell that shows a similar structure to the initial samples without perovskite

Table 3. Impedance fitted characteristics (for batch 1), normalized by masked active area of 0.64 cm^2. The samples 1-4 represent the individual results, whereas the average and their standard deviations are at the end, highlighted with bold.

Name		R_s (Ohm cm^{-2})	R_{ct} (Ohm cm^{-2})	R_{rec} (Ohm cm^{-2})
1	Initial	17.53	66.19	5495
	Revived	20.88	68.55	3430
2	Initial	15.89	71.03	6169
	Revived	19.08	63.22	4456
3	Initial	14.23	52.39	6078
	Revived	24.66	72.80	7558
4	Initial	13.53	51.05	5808
	Revived	18.16	66.27	2252
Average	**Initial**	**15 ± 1**	**60 ± 10**	**5900 ± 300**
	Revived	**21 ± 3**	**68 ± 4**	**4400 ± 2000**

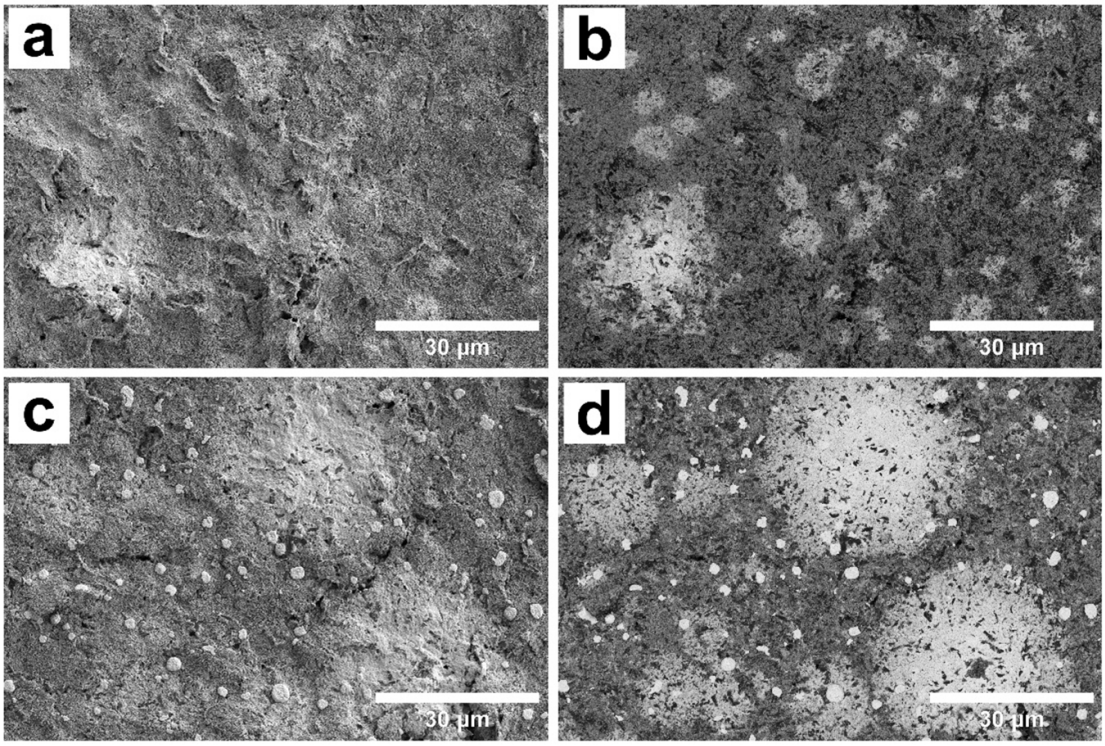

Figure 7. SEM images of initial and revived cells: (a) initial cells ETD; (b) initial cells T1; (c) revived cells ETD; (d) revived cells T1.

forming on the surface. The formation of the perovskite on top of the carbon in some of the samples suggests that a small part of the perovskite nucleates on the surface, likely due to structural changes in the carbon electrode induced by the initial infiltration and revival process. The crystals on top should not interfere with charge transport inside the device. However, it is unknown if they will have an impact, for instance on long term stability of the device.

Figures S2–S4 show the EDS maps for the initial, washed, and revived samples respectively. The atomic percentages obtained from the elemental spectra show a decrease in the amounts of both iodine and lead in the washed sample, indicating that the perovskite was washed out successfully. After revival, the amounts of lead and iodine return to similar values as in the initial sample, indicating that the elemental composition and therefore the amount of perovskite in the revived sample is similar to the initial sample.

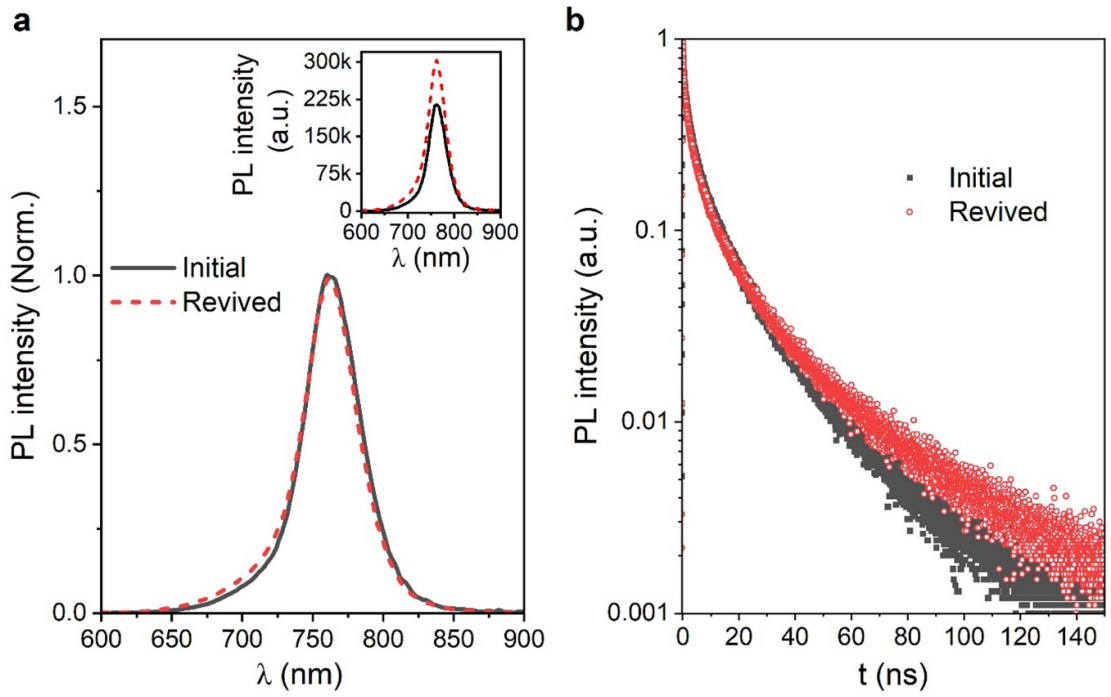

Figure 8. (a) Steady-state and (b) time-resolved photoluminescence (PL and TRPL) spectra of the initial and revived carbon-based perovskite solar cells. Measurements were performed from the glass side using a ∼45° excitation–detection geometry. The excitation wavelength was 405 nm for both PL and TRPL measurements, and the TRPL decay was monitored at an emission wavelength of 760 nm.

To investigate the zirconia underlayer maintains the initial structure after immersion in GVL, we performed SEM analysis on zirconia electrodes (FTO/C-TiO2/M-TiO2/M-ZrO2) before and after GVL immersion (figure S5). The structure remained similar to the initial even after immersion.

To further verify whether the revival step preserved the characteristics of the perovskite absorber, PL and TRPL measurements were performed on the initial and revived devices. When measured from the glass side, both the initial and revived devices showed a broad emission in the 650–850 nm range, with the main peak centered at around 760 nm (figure 8). The normalized PL spectra was almost overlapping, and the absolute PL intensity was also the same order (inset of figure 8). This suggests that the emissive quality of the perovskite layer is largely preserved after revival and that the process does not introduce a strong increase in defect-assisted non-radiative recombination.

The TRPL decay collected at 760 nm also showed very similar behavior for the initial and revived devices, with both traces decaying on the tens-to-hundreds of nanoseconds timescale (figure 8). Since steady-state PL intensity and TRPL lifetime are commonly used as indicators of defect density and recombination losses in perovskite absorbers, the close similarity between the two devices points to a very similar recombination landscape before and after revival. It compares favorably with a recent green-solvent remanufacturing work on mesoscopic carbon perovskite solar cells, where PL peak shifts and shorter TRPL lifetimes were observed when the scaffold or interfaces were more disturbed during recovery (Valadez-Villalobos *et al* 2025). Overall, the PL and TRPL results support that, for the representative devices shown here, the perovskite absorber and its interfaces remain largely intact after revival, which helps explain the nearly unchanged solar cell performance.

3.4. EROI analysis

EROI was utilized to evaluate the influences of the length of the first and second lifetime, together with acceptable degradation and efficiency loss of the cells after revival. In the top right-hand corner of figure 9(a), the maximum achievable EROI is shown (∼23), assuming full retention of performance after revival and same degradation rate during both lifetimes. The maximum indicates that the revived cell, after completing two lifetimes, provided approximately 23 times more electricity than was consumed during the cell's production and revival. Figure 9(a) further illustrates the EROI that can be achieved during varying first and second lifetimes. Thus, looking at the bottom right-hand corner of figure 9(a), the maximum energy return achievable during the first lifetime is 12.3. This is the same as for a single use of the initial cell, highlighted with the white line. Moreover, looking at the area above the bottom

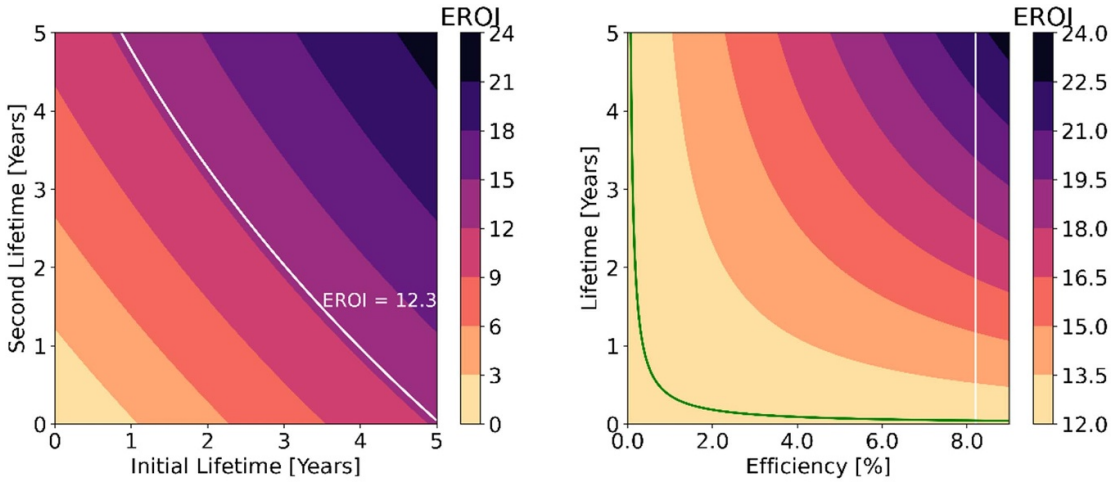

Figure 9. EROI results (a) influence of lifetimes on the EROI performance of revived cells. (white line indicates maximum EROI of the initial cell), assuming average revival efficiency during second-life. (b) Influence of efficiency and lifetime assumptions on the potential EROI (solid line represents the average efficiency of the revived devices) under the 100 mV s^{-1} scanning.

right-hand corner, if the cell lasts 5 years during the first life, it takes a fraction (around 2 d) of the first year for the revived cell to outperform the initial cell. This is due to the revival process consuming far less energy compared to manufacturing (0.4 kWh m^{-2} for revival versus 44.6 kWh m^{-2} for manufacturing). Thus, operating the revived cell for even a short period of time (more than 2 d) at the average efficiency achieved after revival is more beneficial than using two virgin cells from an energy return point of view.

Furthermore, figure 9(a) can be used to optimize the timing of the revival process. For instance, the intersection of the initial lifetime is 4 years with the maximum initial EROI (solid white line) is located in the bottom right-hand part of figure 9(a), at around 1 year. This intersection indicates that if the cell is revived after 4 years, it needs to operate for a year after revival to provide a higher EROI than the initial cell. Similarly, revival after 3 years means operating the revived cell for over 2 years (area in the middle of figure 9(a). Analogically, the entire triangular area below the solid white line depicts lifetime combinations when revival is not justified or should not be pursued. For instance, reviving with first year of initial lifetime would not reach higher EROI than use of single cell for 5 years without revival. However, optimizing the revival period would primarily depend on the degradation of the initial cell and, more importantly, the revived cell. Same degradation rate was assumed before and after revival, yet precise degradation rate after revival needs to be thoroughly investigated. Therefore, the values here are just for initial orientation.

Focusing on figure 9(b), the absolute EROI of the revived cell can be discussed. The EROI increase is visualized by the color gradient and is a function of lifetime and efficiency after revival. Analogous to the previous figure, the top right-hand corner of figure 9(b) shows the maximum achievable EROI. The maximum indicates a case when the initial efficiency can be fully restored. However, a slight decrease in efficiency after revival was discussed above, for which case the real average efficiency after revival is highlighted (solid vertical white line in figure 9(b)). Looking at the intersection of the white line with the top border of the graph, the maximum EROI achieved after the herein discussed revival can be found (EROI = 22.1). Note that this directly corresponds with the maximum EROI in figure 9(a). This indicates that technically 22 times more electricity can be produced over the combined lifetime than was consumed for the manufacturing and revival of the cell. This is approximately twice the value achievable by using two virgin cells, i.e. not reviving, over the same period (which is visualized by the green line, EROI = 12.3). Moreover, other combinations of lifetime and efficiency can be assessed using the same graph. Generally, the area above and to the right of the green line suggests settings at which revival is more beneficial. Thus, it is evident that achieving higher Energy return (compared to not reviving) by reviving the degraded cells is indeed possible.

4. Conclusions

This is the proof-of-concept to establish solvent-based revival of C-PSCs as a practical recycling strategy within the circular economy that combines high efficiency retention with improved sustainability metrics. Solvent-based revival of C-PSCs can achieve near-complete recovery of device performance (95%). Device measurements showed that the *FF* remained stable, while modest reductions in photocurrent density and open-circuit voltage were observed. This highlights that solvent-based revival can maintain the functional integrity of C-PSCs, with remaining limitations attributable to absorber recovery that could be addressed through further optimization. Additionally, the work advances the development of sustainability metrics such as EROI. Our study highlights that the important future research question is exploring carbon electrode composition and architectures to increase both efficiency and mechanical robustness. Indeed, the robustness of carbon scaffolds should be added to the list of desired properties of mesoporous carbon layers.

EIS indicated minor increases in series resistance and charge-transfer resistance at the carbon/perovskite interface, consistent with interfacial modifications induced by the revival process. Importantly, these changes were minor, and impacts to device performance losses were equally minor. Morphological analysis by SEM confirmed that the porous carbon scaffold was preserved, supporting effective reinfiltration of the perovskite precursor. Complementary PL measurements further supported these findings, indicating that revival step preserved the characteristics of the perovskite absorber. From a sustainability perspective, revival offers a clear advantage over manufacturing new devices. EROI calculations revealed that the energy demand of revival is roughly one hundredth of that required for initial production. Which translates into revived cells having a higher return of energy than single-use cells after operating for as short as 2 d. These findings underscore the importance of revival as a viable first level recycling route, complementing existing strategies such as component reuse and material recovery.

Acknowledgments

This work was funded by Research Council of Finland, ECOSOL project (E. A. M.H. and K.M., 347275, S.J. and A.S.A., 347276) E. A. thanks Fortum and Neste Foundation (20210154). M.H. acknowledges SUSMAT profiling funding (Research Council of Finland and University of Turku). S.Y. thanks Circular Materials Bioeconomy Network funded by Ministry of Education and Culture, Finland (CIMANET, Decision No. VN/3137/2024-OKM-6). The MARI infrastructure at the University of Turku was used for this work. We gratefully acknowledge Professor Paola Vivo and Dr G. Krishnamurthy Grandhi (Tampere University, Faculty of Engineering and Natural Sciences, Hybrid Solar Cells) for performing the photoluminescence measurements and for their contributions to the photoluminescence results section of this manuscript.

Data availability statement

All data that support the findings of this study are included within the article (and any supplementary files).

Supporting information available at https://doi.org/10.1088/2631-8695/ae72f6/data1.

Author contributions

Elena S Akulenko 0000-0003-1842-6459
Conceptualization (equal), Investigation (equal), Methodology (equal), Validation (equal), Visualization (equal), Writing – original draft (equal), Writing – review & editing (equal)

Mahboubeh Hadadian 0000-0002-6555-0818
Conceptualization (equal), Data curation (equal), Investigation (equal), Methodology (equal), Supervision (equal), Visualization (equal), Writing – original draft (equal), Writing – review & editing (equal)

Anna Knol 0009-0000-1800-5457
Investigation (equal), Methodology (equal), Validation (equal), Visualization (equal), Writing – original draft (equal), Writing – review & editing (equal)

Simon Jech 0000-0003-3923-7171
Investigation (equal), Methodology (equal), Validation (equal), Visualization (equal), Writing – original draft (equal), Writing – review & editing (equal)

Sirius Yli-Paavola 0009-0000-6432-2402
Investigation (equal), Validation (equal), Visualization (equal), Writing – original draft (equal), Writing – review & editing (equal)

Annukka Santasalo-Aarnio 0000-0003-0077-966X
Conceptualization (equal), Data curation (equal), Funding acquisition (equal), Project administration (equal), Supervision (equal), Writing – review & editing (equal)

Kati Miettunen 0000-0002-6564-6262
Conceptualization (equal), Data curation (equal), Funding acquisition (equal), Investigation (equal), Methodology (equal), Project administration (equal), Supervision (equal), Writing – original draft (equal), Writing – review & editing (equal)

References

2025 National Renewable Energy Laboratory (NREL) best research-cell efficiencies chart—cell-pv-eff
Akulenko E S, Hadadian M, Santasalo-Aarnio A and Miettunen K 2023 Eco-design for perovskite solar cells to address future waste challenges and recover valuable materials *Heliyon* **9** e13584
Akulenko E *et al* 2023 *Bottlenecks in Perovskite Solar Cell Recycling* vol 2023 (EU PVSEC) pp 001–004
Alberola-Borràs J-A, Baker J A, De Rossi F, Vidal R, Beynon D, Hooper K E A, Watson T M and Mora-Seró I 2018 Perovskite photovoltaic modules: life cycle assessment of pre-industrial production process *iScience* **9** 542–51
Arvesen A and Hertwich E G 2015 More caution is needed when using life cycle assessment to determine energy return on investment (EROI) *Energy Policy* **76** 1–6
Barón C, Perpiñán J, Bailera M and Peña B 2023 Techno-economic assessment of glassmaking decarbonization through integration of calcium looping carbon capture and power-to-gas technologies *Sustain. Prod. Consum.* **41** 121–33
Bhandari S, Roy A, Ghosh A, Mallick T K and Sundaram S 2020 Performance of WO_3-incorporated carbon electrodes for ambient mesoscopic perovskite solar cells *ACS Omega* **5** 422–9
Binek A, Petrus M L, Huber N, Bristow H, Hu Y, Bein T and Docampo P 2016 Recycling perovskite solar cells to avoid lead waste *ACS Appl. Mater. Interfaces* **8** 12881–6
Bogachuk D *et al* 2022 Perovskite solar cells with carbon-based electrodes—quantification of losses and strategies to overcome them *Adv. Energy Mater.* **12** 2103128
Bogachuk D *et al* 2024 Remanufacturing perovskite solar cells and modules–a holistic case study *ACS Sustain. Resour. Manage.* **1** 417–26
Celik I, Philips A B, Song Z, Yan Y, Ellingson R J, Heben M J and Apul D 2018 Energy payback time (EPBT) and energy return on energy invested (EROI) of perovskite tandem photovoltaic solar cells *IEEE J. Photovolt.* **8** 305–9
Don M F, Ekanayake P, Jennings J R, Nakajima H, Kumar D U and Lim C M 2023 Influence of metal salts (Al, Ca, and Mg) on the work function and hole extraction at carbon counter electrodes in perovskite solar cells *Heliyon* **9** e17748
García J V *et al* 2024 Simplifying perovskite solar cell fabrication for materials testing: how to use unetched substrates with the aid of a three-dimensionally printed cell holder *R. Soc. Open Sci.* **11** 241012
Gong J, Darling S B and You F 2015 Perovskite photovoltaics: life-cycle assessment of energy and environmental impacts *Energy Environ. Sci.* **8** 1953–68
Grancini G *et al* 2017 One-Year stable perovskite solar cells by 2D/3D interface engineering *Nat. Commun.* **8** 1–8
Hadadian M *et al* 2025 Recycling perovskite solar cells: a green solution-based approach for reviving devices *Proc. Int. Conf. on Hybrid and Organic Photovoltaics (HOPV25)* (https://doi.org/10.29363/nanoge.hopv.2025.137)
Hadadian M, Smått J-H and Correa-Baena J-P 2020 The role of carbon-based materials in enhancing the stability of perovskite solar cells *Energy Environ. Sci.* **13** 1377–407
He J, Bai Y, Luo Z, Ran R, Zhou W, Wang W and Shao Z 2025 Advanced carbon-based rear electrodes for low-cost and efficient perovskite solar cells *Energy Environ. Sci.* **18** 2136–64
Hong L, Hu Y, Mei A, Sheng Y, Jiang P, Tian C, Rong Y and Han H 2017 Improvement and regeneration of perovskite solar cells via methylamine gas post-treatment *Adv. Funct. Mater.* **27** 1703060
Jech Š *et al* 2026 Revive or reuse: environmental and energy insights into mesoporous perovskite solar cells recycling *Sol. Energy Mater. Sol. Cells* **302** 114315
Kadro J M and Hagfeldt A 2017 The end-of-life of perovskite PV *Joule* **1** 29–46
Kerkel F, Markiewicz M, Stolte S, Müller E and Kunz W 2021 The green platform molecule gamma-valerolactone—ecotoxicity, biodegradability, solvent properties, and potential applications *Green Chem.* **23** 2962–76
Ku Z, Xia X, Shen H, Tiep N H and Fan H J 2015 A mesoporous nickel counter electrode for printable and reusable perovskite solar cells *Nanoscale* **7** 13363–8
Larini V *et al* 2025 Circular management of perovskite solar cells using green solvents: from recycling and reuse of critical components to life cycle assessment *EES Sol.* **1** 378–90
Li X *et al* 2025 From lab to market: strategies for stabilizing and scaling perovskite solar cells via printing technologies *Energy Environ. Mater.* **9** e70089
Meng Z, Guo D, Yu J and Fan K 2018 Investigation of Al_2O_3 and ZrO_2 spacer layers for fully printable and hole-conductor-free mesoscopic perovskite solar cells *Appl. Surf. Sci.* **430** 632–8
Miao Y, Ren M, Chen Y, Wang H, Chen H, Liu X, Wang T and Zhao Y 2023 Green solvent enabled scalable processing of perovskite solar cells with high efficiency *Nat. Sustain.* **6** 1465–73

Miettunen K and Santasalo-Aarnio A 2021 Eco-design for dye solar cells: from hazardous waste to profitable recovery *J. Clean. Prod.* **320** 128743
Murphy D J and Hall C A S 2010 Year in review-EROI or energy return on (energy) invested *Ann. New York Acad. Sci.* **1185** 102–18
Pacchioni G 2025 Low-cost recycling of perovskite photovoltaics: solar cells *Nat. Rev. Mater.* **10** 174
Petrov A A, Ordinartsev A A, Fateev S A, Goodilin E A and Tarasov A B 2021 Solubility of hybrid halide perovskites in DMF and DMSO *Molecules* **26** 1–7
Prat D, Hayler J and Wells A 2014 A survey of solvent selection guides *Green Chem.* **16** 4546–51
Radicchi E, Kachmar A, Mosconi E, Bizzarri B, Nunzi F and De Angelis F 2020 Structural and optical properties of solvated PbI_2 in γ-butyrolactone: insight into the solution chemistry of lead halide perovskite precursors *J. Phys. Chem. Lett.* **11** 6139–45
Rong Y, Ku Z, Mei A, Liu T, Xu M, Ko S, Li X and Han H 2014 Hole-conductor-free mesoscopic $TiO_2/CH_3NH_3PbI_3$ heterojunction solar cells based on anatase nanosheets and carbon counter electrodes *J. Phys. Chem. Lett.* **5** 2160–4
Selvanathan V *et al* 2025 Recycling strategies for lead halide perovskite solar cells: current approaches, challenges, and future directions *J. Sci.* **10** 100969
Sengupta A, Afroz M A, Sharma B, Choudhary S, Pant N, Gulia Y, Kalapparambath Rajendra Pai N P, Angmo D and Satapathi S 2025 Commercialization of perovskite solar cells: opportunities and challenges *Sustain. Energy Fuels* **9** 3999–4022
Stevenson J, Sorenson B, Subramaniam V H, Raiford J, Khlyabich P P, Loo Y-L and Clancy P 2017 Mayer bond order as a metric of complexation effectiveness in lead halide perovskite solutions *Chem. Mater.* **29** 2435–44
Väisänen V 2025 Bio-based solvents as alternatives for fossil-based solvents (available at: https://aaltodoc.aalto.fi/handle/123456789/135908)
Valadez-Villalobos K, Worsley C, Garcia-Rodriguez R, Watson T and Davies M 2025 Sustainable remanufacturing of mesoscopic carbon perovskite solar cells using green solvents *RSC Sustain.* **4** 754
Wang K *et al* 2021 "One-key-reset" recycling of whole perovskite solar cell *Matter* **4** 2522–41
Worsley C, Raptis D, Meroni S, Doolin A, Garcia-Rodriguez R, Davies M and Watson T 2021 γ-valerolactone: a nontoxic green solvent for highly stable printed mesoporous perovskite solar cells *Energy Technol.* **9** 1–10
Xiao X *et al* 2025 Aqueous-based recycling of perovskite photovoltaics *Nature* **638** 670–5
Zouhair S, Clegg C, Valitova I, March S, Jailani J M and Pecunia V 2024 Carbon electrodes for perovskite photovoltaics: interfacial properties, meta-analysis, and prospects *Sol. RRL* **8** 2300929